

# Jahn-Teller Distortions and the Supershell Effect in Metal Nanowires

D. F. Urban<sup>1</sup>, J. Bürki<sup>1,2</sup>, C.-H. Zhang<sup>2</sup>, C. A. Stafford<sup>2</sup>, and Hermann Grabert<sup>1</sup>

<sup>1</sup>*Physikalisches Institut, Albert-Ludwigs-Universität, D-79104 Freiburg, Germany*

<sup>2</sup>*Department of Physics, University of Arizona, Tucson, AZ 85721*

(Dated: June 28, 2018)

A stability analysis of metal nanowires shows that a Jahn-Teller deformation breaking cylindrical symmetry can be energetically favorable, leading to stable nanowires with elliptic cross sections. The sequence of stable cylindrical and elliptical nanowires allows for a consistent interpretation of experimental conductance histograms for alkali metals, including both the electronic shell and supershell structures. It is predicted that for gold, elliptical nanowires are even more likely to form since their eccentricity is smaller than for alkali metals. The existence of certain metastable “superdeformed” nanowires is also predicted.

PACS numbers: 71.70.Ej, 73.21.Hb, 68.65.La, 47.20.Dr

The effects of shell filling on the abundance spectra of metal clusters have been known for years and explain the existence of clusters with “magic numbers,” corresponding to full electronic shells, which are observed more frequently than others [1]. More recently, electronic shell and supershell structures in alkali metal nanowires have been reported by the Leiden group [2, 3, 4]. The conductance  $G$  was recorded during the breaking of nanowires in a mechanically controllable break junction (MCBJ), and histograms were built out of thousands of measurements. When the temperature is large enough to allow the wire to explore the phase space of possible shapes, the shell structure shows up as peaks in the histogram of  $\sqrt{G}$  that are equally spaced, while the supershell structure manifests itself as a modulation of the amplitude of the peaks (See Agraït *et al.* [5] for a recent review).

The electron-shell structure in alkali nanowires can be understood qualitatively using the free-electron model of a cylinder [2]. However, more detailed stability analyses of axisymmetric wires [6, 7, 8] have revealed a sequence of stable “magic” radii, with characteristic gaps that are not fully consistent with the nearly perfect periodicity of the experimentally observed peak positions. The deviations can be accounted for neither by the inclusion of disorder [9], nor by the use of more elaborate self-consistent jellium models [10]. Since gaps in the sequence of cylindrical nanowires arise from a degeneracy of conductance channels, it is natural to assume that a Jahn-Teller deformation breaking the symmetry can lead to more stable deformed configurations.

While the experimental manifestations of electron-shell structure are similar in metal clusters and nanowires, the Jahn-Teller effect plays out quite differently in these two systems. Metal clusters and nanowires differ fundamentally in that surface effects tend to stabilize clusters, while they lead to a Rayleigh instability in nanowires [6]. As a result, Jahn-Teller deformations of clusters are very common and typically rather small [11, 12] while, as we show here, they only occur for a minority of nanowires and can be rather large. Nevertheless, there are several

stable nanowires with elliptic cross-sections (referred to as *elliptical nanowires* henceforth), leading to a sequence of stable cylindrical and elliptical nanowires that allows for a satisfying interpretation of the experiments on electronic shell and supershell structure [2, 3, 4]. In addition, our theory predicts the existence of short-lived superdeformed wires.

We use a nanoscale free-electron model, treating the electrons as a non-interacting Fermi gas confined within the wire by hard-wall boundary conditions [13]. This continuum model is especially suitable for alkali metals, but can also be applied to other monovalent metals. Macroscopic arguments [7] suggest that the surface tension  $\sigma_s$  should drive a crossover from a crystalline solid to a plastic or fluid below a critical radius  $R_{\min} = \sigma_s/\sigma_Y$ , where  $\sigma_Y$  is the yield strength. Typically,  $R_{\min} \sim 10$  nm in metals [7]. This implies that electronic effects should dominate over atomistic effects for sufficiently small radii. Indeed, a crossover from atomic-shell to electron-shell effects with decreasing radius is observed in both metal clusters [14] and nanowires [4, 15, 16, 17], justifying *a posteriori* the use of the nanoscale free-electron model in the later regime.

Guided by evidence of the existence of non-spherical clusters [11, 12], we consider straight elliptical nanowires [18] aligned along the  $z$ -axis. The wire cross-section is characterized by the ellipse’s two major semi-axes  $a$  and  $b$ , or equivalently, by the area parameter  $\sigma^2 = a \cdot b$  and the aspect ratio  $\varepsilon = a/b$ . When a small perturbation, written as a Fourier series, is added to a wire of length  $L$ , the geometry is characterized by the two functions

$$\begin{aligned}\sigma(z) &= \bar{\sigma} + \lambda \sum_q \sigma_q e^{iqz} \equiv \bar{\sigma} + \lambda \delta\sigma(z), \\ \varepsilon(z) &= \bar{\varepsilon} + \lambda \sum_q \varepsilon_q e^{iqz} \equiv \bar{\varepsilon} + \lambda \delta\varepsilon(z),\end{aligned}\quad (1)$$

where the dimensionless parameter  $\lambda$  sets the size of the perturbation. The perturbation wave vector  $q$  must be an integer multiple of  $2\pi/L$  and, since  $\sigma(z)$  and  $\varepsilon(z)$  are real, we have  $\sigma_{-q} = \sigma_q^*$  and  $\varepsilon_{-q} = \varepsilon_q^*$ . The deformation

must fulfill another constraint which comes from the fact that, depending on material parameters, the deformed wire tries to find a compromise between a volume conserving deformation and one ensuring electroneutrality [19]. Here we use the general constraint

$$\mathcal{N} \equiv k_F^3 \mathcal{V} - \eta(3\pi k_F^2 \mathcal{A}/8) = \text{const}, \quad (2)$$

where  $\mathcal{V}$  is the volume of the wire,  $\mathcal{A}$  its surface area, and  $k_F = 2\pi/\lambda_F$  the Fermi wavevector. The parameter  $\eta$  can be adjusted so as to fix the value of the effective surface tension to the material-specific value. In particular,  $\eta = 0$  corresponds to a constant-volume constraint, and  $\eta = 1$  is the constraint of constant (zero temperature) Weyl charge.

A nanowire is an open system, with electrons being injected and absorbed by the leads, so that we need to calculate its grand canonical potential  $\Omega$  in order to determine the energetic cost of a deformation. A fully quantum mechanical stability analysis of cylindrical nanowires [8] shows that, if the wires are short enough, and/or the temperature is not too low, their stability is essentially determined by their response to long wavelength perturbations. For these we can use the adiabatic approximation and decouple the transverse and longitudinal motions yielding a series of effectively one-dimensional problems, which can be solved with the WKB approximation, in which  $\Omega$  is given by [13]

$$\Omega[T, L; \sigma, \varepsilon] = \int_0^\infty dE \left( -\frac{\partial f}{\partial E} \right) \Xi[E, L; \sigma, \varepsilon], \quad (3)$$

$$\Xi[E, L; \sigma, \varepsilon] = -\frac{8E_F}{3\lambda_F} \int_0^L dz \sum_\nu \left( \frac{E - E_\nu(\sigma, \varepsilon)}{E_F} \right)^{3/2} \quad (4)$$

Here  $f = (1 + \exp[(E - E_F)/k_B T])^{-1}$  is the Fermi function at temperature  $T$ ,  $E_F$  is the Fermi energy, and the  $E_\nu$ 's are the transverse eigenenergies. The sum in Eq. (4) runs over all open channels  $\nu$ , for which  $E_\nu(\sigma, \varepsilon) < E$ . A factor of 2 accounts for spin degeneracy. Note that at zero temperature Eq. (3) reduces to  $\Omega[T=0, L] = \Xi[E_F, L]$ .

The transverse eigenenergies can be written as  $E_\nu(\sigma, \varepsilon) = E_F \frac{\gamma_\nu(\varepsilon)^2}{(k_F \sigma)^2}$ , where the  $\gamma_\nu$ 's are the zeros of the modified Mathieu functions [20], and can be computed numerically. In the limit  $\varepsilon \rightarrow 1$ , we recover the result for a cylindrical wire, where most eigenenergies are degenerate. As shown in Fig. 1, this degeneracy is lifted for  $\varepsilon \neq 1$  as a result of the decrease in symmetry, so that an elliptic nanowire can sometimes be more stable than the axisymmetric one, leading to a Jahn-Teller deformation.

The energetic cost of a small deformation of a straight elliptical nanowire can be calculated by expanding Eq. (3) as a series in the parameter  $\lambda$ ,

$$\Omega = \Omega^{(0)} + \lambda \Omega^{(1)} + \lambda^2 \Omega^{(2)} + \mathcal{O}(\lambda^3). \quad (5)$$

A nanowire  $(\bar{\sigma}, \bar{\varepsilon})$  is energetically stable at temperature  $T$  if  $\Omega^{(1)}(\bar{\sigma}, \bar{\varepsilon}) = 0$  and  $\Omega^{(2)}(\bar{\sigma}, \bar{\varepsilon}) > 0$  for every possible deformation  $(\delta\varepsilon, \delta\sigma)$  satisfying  $\partial\mathcal{N} = 0$ .

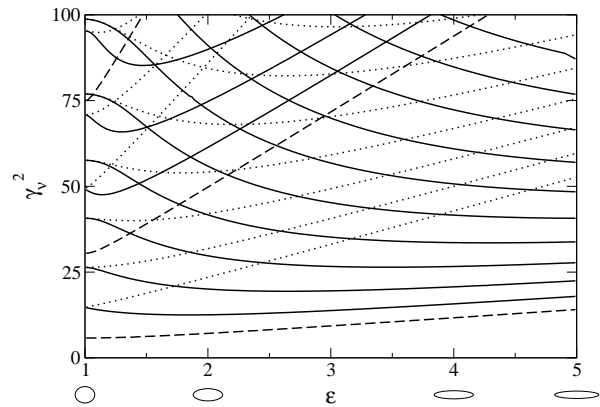


FIG. 1: Eigenenergies of a 2d electron gas confined to an elliptical shape as a function of the aspect ratio  $\varepsilon$ . Solid and dotted lines indicate even and odd states respectively, while states non-degenerate at  $\varepsilon=1$  are shown with a dashed line.

The expansion of Eq. (4) yields

$$\frac{\lambda_F}{L} \Xi^{(0)} = -\frac{8}{3\sqrt{E_F}} \sum_\nu [E - \bar{E}_\nu]^{3/2}, \quad (6)$$

$$\frac{\lambda_F}{L} \Xi^{(1)} = \frac{8}{\sqrt{E_F}} \sum_\nu \bar{E}_\nu \sqrt{E - \bar{E}_\nu} \left( \frac{\bar{\gamma}'_\nu}{\bar{\gamma}_\nu} \varepsilon_0 - \frac{\sigma_0}{\bar{\sigma}} \right), \quad (7)$$

$$\frac{\lambda_F}{L} \Xi^{(2)} = \frac{4}{\sqrt{E_F}} \sum_q \begin{pmatrix} \sigma_q/\bar{\sigma} \\ \varepsilon_q \end{pmatrix}^\dagger \begin{pmatrix} A_{\sigma\sigma} & A_{\sigma\varepsilon} \\ A_{\varepsilon\sigma} & A_{\varepsilon\varepsilon} \end{pmatrix} \begin{pmatrix} \sigma_q/\bar{\sigma} \\ \varepsilon_q \end{pmatrix}, \quad (8)$$

where  $\bar{E}_\nu = E_\nu(\bar{\sigma}, \bar{\varepsilon})$ , and  $\bar{\gamma}_\nu = \gamma_\nu(\bar{\varepsilon})$ . The prime indicates differentiation with respect to  $\varepsilon$ . The elements of the matrix  $A$  in Eq. (8) are given by

$$\begin{aligned} A_{\sigma\sigma} &= \sum_\nu \bar{E}_\nu \left( 3\sqrt{E - \bar{E}_\nu} - \frac{\bar{E}_\nu}{\sqrt{E - \bar{E}_\nu}} \right), \\ A_{\sigma\varepsilon} &= \sum_\nu \bar{E}_\nu \left[ \left[ \frac{\bar{\gamma}'_\nu}{\bar{\gamma}_\nu} \right]^2 + \frac{\bar{\gamma}''_\nu}{\bar{\gamma}_\nu} \right] \sqrt{E - \bar{E}_\nu} - \left[ \frac{\bar{\gamma}'_\nu}{\bar{\gamma}_\nu} \right]^2 \frac{\bar{E}_\nu}{\sqrt{E - \bar{E}_\nu}}, \\ A_{\varepsilon\varepsilon} &= -\sum_\nu \bar{E}_\nu \frac{\bar{\gamma}'_\nu}{\bar{\gamma}_\nu} \left( 2\sqrt{E - \bar{E}_\nu} - \frac{\bar{E}_\nu}{\sqrt{E - \bar{E}_\nu}} \right). \end{aligned} \quad (9)$$

The constraint  $\partial\mathcal{N} = 0$  on allowed deformations restricts the number of independent Fourier coefficients in Eq. (1). Hence we can express  $\sigma_0$  in terms of the other coefficients and expand it as a series in  $\lambda$ ,

$$\sigma_0 = \sigma_0^{(0)}(\bar{\varepsilon}, \bar{\sigma}, \varepsilon_0) + \lambda \sigma_0^{(1)}(\bar{\varepsilon}, \bar{\sigma}, \{\varepsilon_q, \sigma_q\}) + \mathcal{O}(\lambda^2), \quad (10)$$

and eliminate  $\sigma_0$  from Eqs. (7) and (8), modifying the expressions for  $\Xi^{(1)}$  and the stability matrix  $A$ . At zero temperature, the modified condition  $\tilde{\Xi}^{(1)} = 0$  determines which wires are stationary states, while the positivity of the modified matrix  $\tilde{A}$  reveals the stability of the wire. The results for finite temperature can be derived analogously by evaluating Eq. (3) numerically.

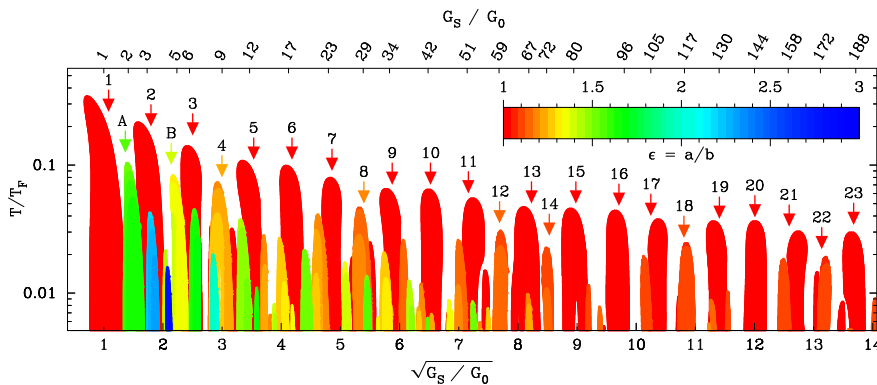


Figure 2 shows the stable geometries as a function of temperature and conductance, with the surface tension adjusted to the value 0.22 N/m (i.e.  $\eta = 0.93$ ), corresponding to Na [21]. The color represents the value of the aspect ratio  $\varepsilon$  and the  $x$ -axis is given by the square root of the corrected Sharvin conductance  $G_S = G_0(k_F^2\sigma^2/4 - k_F\mathcal{P}/4\pi + 1/6)$ . Here  $G_0 = 2e^2/h$  is the conductance quantum and  $\mathcal{P}$  the ellipse perimeter.

The possibility to observe a stable wire in conductance histograms depends mostly on two conditions: (i) The wire has to be formed often enough to be statistically relevant; (ii) It needs to have a long enough lifetime so as to be recorded. Condition (i) depends on the ability of the system to probe new configurations, which is determined by the mobility of the atoms and the density of stable geometries in configuration space. Regarding point (ii), a calculation of the lifetime of a nanowire is beyond the scope of this paper, but one can expect that wires that are linearly stable up to larger temperatures  $T_{max}$  will have longer lifetimes at low temperatures [22].

Based on these considerations, we extract the most stable configurations from Fig. 2, defined as the geometries that persist up to the highest temperature compared to their neighboring configurations. Those wires are marked with numbered arrows in Fig. 2. For each stability peak, we extract its mean Sharvin conductance and its width, and plot them as a function of the peak number in Fig. 3, together with the experimental data from Ref. [2]. Note that the striking fit is only possible when including elliptical nanowires, for which the corresponding aspect ratios  $\varepsilon$  are also shown in Fig. 3.

The heights of the dominant stability peaks in Fig. 2 exhibit a periodic modulation, with minima occurring at peaks 4, 8, 12, 18, etc. The positions of these minima are in perfect agreement with the observed supershell structure in conductance histograms of alkali metal nanowires [3]. Interestingly, the nodes of the supershell structure, where the shell effect for a cylinder is suppressed, are precisely where the most stable elliptical nanowires are predicted to occur. Thus the Jahn-Teller distortions and the supershell effect are inextricably linked.

While both the shell [2] and supershell [3] effects are accurately described by our stability analysis, our ther-

modynamic model does not directly address the complex dynamical process by which various contact structures form in MCBJ experiments, and therefore cannot describe every detail of the conductance histograms, such as their highly non-trivial temperature dependence.

Our stability analysis also reveals two highly deformed elliptical nanowires with conductance values of  $2G_0$  and  $5G_0$ , marked in Fig. 2 by arrows A and B, respectively. They are expected to appear more rarely due to their reduced stability relative to the neighboring peaks, and their large aspect ratio  $\varepsilon$  (see Table I) that renders them rather isolated in configuration space [23]. Conductance histograms of the alkali metals often do show a conductance peak at  $5G_0$  and a shallow shoulder at  $2G_0$  [2, 4]. Nevertheless, these peaks were *not included* in the experimental analysis of shell structure in Refs. 2 and 4. Note that the definition of an experimental “peak” depends on the selection criteria and smoothing of the data.

Of the three alkali metals, Li, Na and K, Potassium has the lowest and Lithium the highest melting temperature. This suggests that at a given temperature the mobility of the atoms is highest in K and lowest in Li. This is reflected in the fact that the evidence of the highly deformed nanowires A and B is clear for K, can be seen for Na, but is barely visible for Li [4].

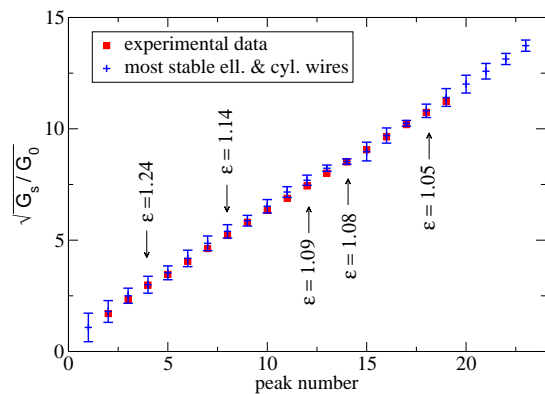


FIG. 3: (color online) Comparison of the experimental shell structure for Na (taken from Ref. [2]) with our theoretical predictions of the most stable Na nanowires. Elliptical wires are labeled with the corresponding aspect ratio  $\varepsilon$ .

	$G_S/G_0$	$\varepsilon^{(\text{Na})}$	$k_B T_{\text{max}}^{(\text{Na})}$ [eV]	$\varepsilon^{(\text{Au})}$	$k_B T_{\text{max}}^{(\text{Au})}$ [eV]
A	2.3	1.65	0.360	1.50	0.376
B	5.3	1.32	0.282	1.27	0.326
4	9.0	1.24	0.243	1.17	0.288
8	29.1	1.14	0.152	1.12	0.194
12	59.2	1.09	0.100	1.08	0.122
14	72.8	1.08	0.076	1.07	0.083
18	116.2	1.05	0.081	1.05	0.105

TABLE I: Most stable elliptical nanowires (with  $\varepsilon > 1$ ) for Na and Au. Listed are the labels from Fig. 2, the mean Sharvin conductance  $G_S$ , the aspect ratio  $\varepsilon$ , and the maximum temperature  $T_{\text{max}}$  up to which the wires remain stable, which is related to the depth of the corresponding energetic minimum.

In addition to wire A, Fig. 2 shows a number of “superdeformed” nanowires with  $\varepsilon > 1.5$ . The most stable are at  $(G, \varepsilon) = (2, 1.65), (3, 2.25), (4, 2.8), (6, 1.65), (8, 2.0), (12, 1.65), (19, 1.55), (29, 1.55)$  and  $(41, 1.6)$ . An aspect ratio near 2 is favorable for the shell effect [24], as evidenced by the large gaps in the energy spectrum (Fig. 1), but the large cost in surface energy renders these wires less stable than the magic cylindrical wires and the “normal-deformed” wires listed in Table I.

Conductance histograms have also been recorded for gold, both at low [25] and room temperatures [15, 16, 17], where evidence of electronic shell effects has been reported. Although the explanation of some features of Au wires, e.g. surface reconstruction, requires explicit inclusion of 5d-orbitals, the jellium model is sufficient to explain electron-shell effects. Performing a stability analysis for gold requires adjusting the deformation constraint (2) according to the surface tension for Au, ( $1.3 \text{ N/m}$  [21],  $\eta = 0.61$ ), which is higher than for Na. Therefore the results are somewhat different: Stable configurations appear at the same conductance values, but the temperature  $T_{\text{max}}$  up to which elliptical wires remain stable is larger, and these wires are less deformed than for Na (see Table I). As a consequence, the probability to observe elliptical nanowires in experiments is enhanced. Indeed, several experimental histograms [15, 25] for Au show clear peaks at conductance values of  $2 G_0$  and  $5 G_0$ .

In conclusion, we have presented a stability analysis of elliptical metal nanowires, using a jellium model, and have shown that Jahn-Teller-distorted wires can be stable. The derived sequence of stable cylindrical and elliptical geometries explains the experimentally observed shell and supershell structures for alkali metals. Deformed wires can explain additional conductance peaks observed in alkali metals and gold.

We are grateful to J. van Ruitenbeek for sharing his data on Na conductance histograms. This research has been supported by the DFG through SFB 276 and the EU Network DIENOW. CHZ and CAS acknowledge support from NSF grant DMR0312028.

- [1] W. A. Heer, Rev. Mod. Phys. **65**, 611 (1996).
- [2] A. I. Yanson, I. K. Yanson, and J. M. van Ruitenbeek, Nature **400**, 144 (1999).
- [3] A. I. Yanson, I. K. Yanson, and J. M. van Ruitenbeek, Phys. Rev. Lett. **84**, 5832 (2000).
- [4] A. I. Yanson, I. K. Yanson, and J. M. van Ruitenbeek, Low Temp. Phys. **27**, 807 (2001).
- [5] N. Agraït, A. Levy Yeyati, and J. M. van Ruitenbeek, Phys. Rep. **377**, 81 (2003).
- [6] F. Kassubek, C. A. Stafford, H. Grabert, and R. E. Goldstein, Nonlinearity **14**, 167 (2001).
- [7] C.-H. Zhang, F. Kassubek, and C. A. Stafford, Phys. Rev. B **68**, 165414 (2003).
- [8] D. F. Urban and H. Grabert, Phys. Rev. Lett. **91**, 256803 (2003).
- [9] J. Bürki and C. A. Stafford, in *Electronic Correlations: From Meso- to Nano-Physics*, edited by T. Martin, G. Montambaux, and J. Tran Thanh Van (EDP Sciences, Les Ulis, France, 2001), pp. 27–30.
- [10] M. J. Puska, E. Ogando, and N. Zabala, Phys. Rev. B **64**, 033401 (2001).
- [11] A. Bulgac and C. Lewenkopf, Phys. Rev. Lett. **71**, 4130 (1993).
- [12] M. Schmidt, C. Ellert, W. Kronmüller, and H. Haberland, Phys. Rev. B **59**, 10970 (1999).
- [13] C. A. Stafford, D. Baeriswyl, and J. Bürki, Phys. Rev. Lett. **79**, 2863 (1997).
- [14] T. P. Martin, Phys. Rep. **273**, 199 (1996).
- [15] M. Díaz, J. L. Costa-Krämer, E. Medina, A. Hasmy, and P. A. Serena, Nanotechnology **14**, 113 (2003).
- [16] E. Medina, M. Díaz, N. León, C. Guerrero, A. Hasmy, P. A. Serena, and J. L. Costa-Krämer, Phys. Rev. Lett. **91**, 026802 (2003).
- [17] A. I. Mares, A. F. Otte, L. G. Soukiassian, R. H. M. Smit, and J. M. van Ruitenbeek, Phys. Rev. B **70**, 073401 (2004).
- [18] Higher-order multipole deformations are also possible, but cost significantly more surface energy. They are therefore only expected to occur at low conductance.
- [19] C. A. Stafford, F. Kassubek, J. Bürki, and H. Grabert, Phys. Rev. Lett. **83**, 4836 (1999).
- [20] M. van den Broek and F. M. Peeters, Physica E **11**, 345 (2001).
- [21] W. R. Tyson and W. A. Miller, Surf. Sci. **62**, 267 (1977).
- [22] Recent calculations for axisymmetric wires [26] confirm this for neighboring peaks, but show that the relative lifetimes of wires with very different conductances cannot be directly inferred from  $T_{\text{max}}$ .
- [23] A nanowire produced by pulling apart an axisymmetric contact has a smaller probability to transform into a highly deformed configuration than into a neighboring cylindrical configuration.
- [24] P. J. Nolan and P. J. Twin, Ann. Rev. Nucl. Part. Sci. **38**, 533 (1988).
- [25] J. L. Costa-Krämer, N. García, and H. Olin, Phys. Rev. B **55**, 12910 (1997).
- [26] J. Bürki, C. A. Stafford, and D. L. Stein, in *Noise in Complex Systems and Stochastic Dynamics II*, edited by Z. Gingl et al. (SPIE Proceedings, 2004), vol. 5471, pp. 367–379.